Aeroelastic Analysis through Non-Linear Beam Finite Elements with Bending-Torsion Coupling Formulation

AIAA SciTech Forum
8-12 January 2024, Orlando, FL
AIAA SCITECH 2024 Forum

10.2514/6.2024-1073

Aeroelastic Analysis through Non-Linear Beam Finite Elements with Bending-Torsion Coupling Formulation

Cesare Patuelli[1], Enrico Cestino[2] and Giacomo Frulla[3]
DIMEAS, Politecnico di Torino, Corso Duca degli Abruzzi 24, 10129 Torino, Italy.

This research paper presents a procedure for static aeroelastic analysis of high aspect-ratio composite wings. The structural analysis is performed through the finite element method coupled with an aerodynamic analysis based on the vortex lattice method. The finite element model is obtained with beam finite elements with bending-torsion coupling formulation, which allows to consider the material coupling given by oriented anisotropic material. An advanced formulation of the same beam element can be used to consider geometric non-linearities. An iterative procedure computes the aerodynamic loads acting on the initially undeformed structures, then the obtained deformation is used to compute the aerodynamic loads for the deformed configuration until convergence. The aeroelastic analysis can be repeated for different speeds to find the divergence speed. This procedure has been tested on previously published analytical and experimental results on composite structures with different layups showing good accordance. Moreover, curvilinear lamination has been considered for the analysis to show the effects on the static aeroelastic performance.

I. Nomenclature

C_{ij}	=	Stiffness coefficient
GJ_t	=	Torsional stiffness
EI_y	=	Out-of-plane bending stiffness coefficient
Ez	=	In-plane bending stiffness coefficient
m	=	Mass
t	=	Time
v	=	In-plane displacement component
x	=	Spatial coordinate
w	=	Out-of-plane displacement component
φ	=	Axial rotation component
ρ	=	Material Density
I_p	=	Polar moment of inertia
θ_y	=	Out-of-plane rotation component
θ_z	=	In-plane rotation component
L	=	Element length
ρ_i	=	Curvature
M_i	=	Resultant moment
E_T	=	Young tensile modulus
ν_{LT}	=	Poisson coefficient
G_{LT}	=	Shear Modulus
l	=	Beam length
D_{ij}	=	Flexural modulus

[1] PhD Student, cesare.patuelli@polito.it
[2] Associate Professor, enrico.cestino@polito.it
[3] Associate Professor, giacomo.frulla@polito.it

$Q_{ij}^{(\theta_k)}$ = Off-axis lamina modulus
θ_k = Ply angle of the kth ply
z_k = Distance up from the midplane to the upper surface of the *k*th ply
t = Lamina total thickness
Cl_α = Lift curve slope
Cl_{α_r} = Reduced lift curve slope
θ_1 = Fiber orientation at the first section of the beam
θ_2 = Fiber orientation at the end section of the beam

II. Introduction

A current trend in aviation is toward the use of high aspect ratio wing structures with the scope of improving efficiency and reducing structural weight. The resulting slender structures are highly flexible and the large deformations can introduce nonlinear structural effects that affect the aeroelastic properties of the structure [1]–[4]. Divergence is a typical aeroelastic instability involving torsion deformation which can potentially increase and become critical. Bending-torsion flutter is an aeroelastic dynamic instability that causes increasing amplitude oscillation and can become dangerous for structural integrity. Non-linear effects can sensibly affect the aeroelastic properties of a structure [5] and therefore must be accounted for during the early design stages. Patil et. al [6] studied the effect of structural geometric non-linearities on the flutter behavior of high aspect-ratio wings and observed a significant change in structural frequencies and a reduction of the flutter speed. Sherrer et al. [7] used aeroelastic tailoring to increase the divergence speed of a composite forward-swept wing and validated the results through low-speed tunnel tests. Guo [8] demonstrated aeroelastic tailoring to significantly reduce the weight of aircraft structures and increase up to 30% of the flutter speed. Librescu and Song [9] adopted a thin-walled anisotropic composite beam model to study the sub-critical static aeroelastic response and the divergence instability of swept-forward aircraft wing structures. Li et al. [10] presented a rapid computational fluid dynamics-based aeroelastic tool that used a reduced order model for aerodynamics that is updated for any modification of the structure by using the structural dynamics reanalysis method.

Coupled computational fluid dynamics and finite element method formulation for aeroelastic analysis can be used for detailed simulations [11]. These models are generally very advanced and usually require a large computational power which is not efficient for early design stage optimizations. For this reason, low-order structural models can help to reduce the computational cost and guarantee similar accuracy for preliminary optimizations. Geometrically exact beam formulation is a popular approach [11], [12] and has been used in several works for highly deformed wing structure analysis. Drela [13] used beam elements with non-linear formulation to develop an aerodynamic and structural simulation model for flexible aircraft, while Patil [3] presented a theory for flight-dynamic analysis of highly flexible wing configurations accounting for geometric non-linearities. More recently, a new class of low-order structural models relying on high-order modal expansion has been developed [14], [15]. However, these models require non-linear static responses of a Finite Element Model (FEM) to identify modal expansion terms.

Anisotropic materials can be adopted to enhance the aeroelastic performances of wing box structures according to the concept of aeroelastic tailoring [16], [17]. This technique demonstrates important advantages when combined with composite material where the lay-ups can be optimized to mitigate the aeroelastic phenomena. Other aeroelastic tailoring techniques involve functionally graded materials [18]–[20], variable angle tow [21], [22], or curvilinear stiffener panels [23], [24]. Aeroelastic tailoring relies on the structural couplings introduced with a specific orientation of composite fibers or stiffeners to modify the aeroelastic properties of a wing structure. The optimization of these structures can be very demanding in terms of time and computational costs, for this reason, equivalent models with beam finite elements can be adopted during early design stages. The problem encouraged the development of aeroelastic prediction methods that account for the nonlinear effects on highly flexible structures [25]–[27], but the introduction of a nonlinear beam finite elements that account for the material bending torsion coupling could be a benefit for this class of analysis.

Recently, a beam finite element with bending torsion coupling formulation (BTCE) has been developed for static and dynamic analysis [28] and validated through experimental modal analysis [29]. The results demonstrated good accuracy and performance, moreover, its capabilities as an optimization tool have been demonstrated in [30] where the element has been employed to find the best configuration with prescribed constraints on deformations and bending-torsion couplings. The beam finite element has been further developed by introducing a nonlinear formulation, where

the nonlinear stiffness matrix is derived with a perturbation approach. The derivation of the nonlinear beam finite element and its experimental validation are part of a research paper currently under review.

This study aims to expand the application of the derived finite element to aeroelastic analysis with a coupled aerodynamic and structural model. An aeroelastic analysis procedure has been developed to efficiently compute the deformation induced by aerodynamic loads on composite wing structures. This procedure accounts for the variation of aerodynamic loads caused by the deformation of the structure. The aerodynamic loads are initially computed for the undeformed structure and then applied to the structural model. The deformed configuration is then introduced in the aerodynamic model to obtain the corresponding aerodynamic loads. The process is iterated until convergence or divergence. The procedure has been tested on composite plates presented in [31] showing good accordance for the divergence speed obtained with the present procedure and the analytical and experimental results. Moreover, the aeroelastic analysis has been performed on composite plates with curvilinear lamination to analyze the effects on the aeroelastic performance.

III. Bending-Torsion Coupling beam finite Element (BTCE)

This section presents the BTCE used in this research work for structural analysis. The BTCE has been derived by Patuelli et al. [28] and validated with experimental and numerical results for static and dynamic analysis [29]. More recently the optimal curvilinear path of panel stiffeners has been determined through a BTCE model implemented in an optimization algorithm [30]. The BTCE has been derived through Galerkin's method and with the hypothesis of constant torsional moment along the element length. The derivation starts with the equation of motion derived according to [32]–[34] and reported in Equation (1). The terms C_{ij} are the stiffness coefficient which can be redefined with the convention that $C_{11} = GJ_t$, $C_{22} = EI_y$, $C_{33} = EI_z$, and $C_{12} = K$. Particular attention must be paid to the coupling term K which links the torsional rotation φ with the out-of-plane deflection w, while the in-plane deflection v is independent. The approximating functions are reported in Equation (2) with the components of the shape functions within square brackets associeated to the nodal degrees of freedome of a two node beam element represented in Figure 1.

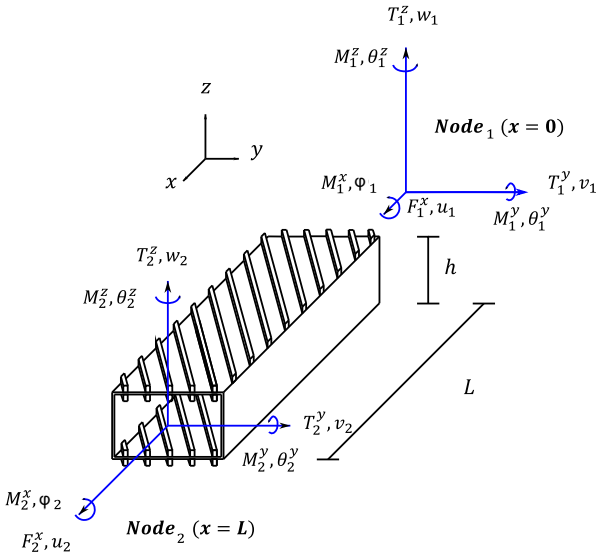

Fig. 1 Beam finite element reference system [28]

$$\begin{cases} \mathrm{m}\dfrac{\partial^2 v}{\partial t^2} + C_{33}\dfrac{\partial^2}{\partial x^2}\left(\dfrac{\partial^2 v}{\partial x^2}\right) = 0 \\ \mathrm{m}\dfrac{\partial^2 w}{\partial t^2} + C_{22}\dfrac{\partial^2}{\partial x^2}\left(\dfrac{\partial^2 w}{\partial x^2}\right) - C_{12}\dfrac{\partial}{\partial x}\left(\dfrac{\partial^2 \varphi}{\partial x^2}\right) = 0 \\ \rho I_p \dfrac{\partial^2 \varphi}{\partial t^2} - C_{11}\dfrac{\partial}{\partial x}\left(\dfrac{\partial \varphi}{\partial x}\right) + C_{12}\dfrac{\partial}{\partial x}\left(\dfrac{\partial^2 w}{\partial x^2}\right) = 0 \end{cases} \tag{1}$$

$$\begin{aligned} v(x) &= \left[1 - \frac{3x^2}{L^2} + \frac{2x^3}{L^3}\right] v_1 + \left[x - \frac{2x^2}{L} + \frac{x^3}{L^2}\right] \theta_1^z + \left[\frac{3x^2}{L^2} - \frac{2x^3}{L^3}\right] v_2 + \left[-\frac{x^2}{L} + \frac{x^3}{L^2}\right] \theta_2^z \\ w(x) &= \left[1 - \frac{3x^2}{L^2} + \frac{2x^3}{L^3}\right] w_1 - \left[x - \frac{2x^2}{L} + \frac{x^3}{L^2}\right] \theta_1^y + \left[\frac{3x^2}{L^2} - \frac{2x^3}{L^3}\right] w_2 - \left[\frac{x^2}{L} + \frac{x^3}{L^2}\right] \theta_2^y \\ \varphi(x) &= \left[1 - \frac{x}{L}\right] \varphi_1 + \left[\frac{6K}{GJ_t L^3}(x^2 - Lx)\right] w_1 + \left[\frac{3K}{GJ_t L^2}(Lx - x^2)\right] \theta_1^y + \left[\frac{x}{L}\right] \varphi_2 + \left[\frac{6K}{GJ_t L^3}(Lx - x^2)\right] w_2 \\ &\quad + \left[\frac{3K}{GJ_t L^2}(Lx - x^2)\right] \theta_2^y \end{aligned} \tag{2}$$

The residual functions can be written from Equation (1). Integrating over the element length the product of the residual functions times the shape functions and imposing the result equal to 0, the stiffness matrix can be obtained. The detailed procedure is presented in [28]. The stiffness matrix [K] is reported in Appendix A.

IV. Non-Linear BTCE

V.

The beam finite element presented in the previous section has been further improved including the non-linear terms in the stiffness matrix derivation to perform static and dynamic analysis in the presence of geometric non-linearities. In this case, the stiffness matrix was obtained with Hamilton's Principle reported in Equation (3).

$$\partial\pi = \int_0^L (M_1 \partial\rho_1 + M_2 \partial\rho_2 + M_3 \partial\rho_3) ds = 0 \tag{3}$$

With the moments resultants expressed by Equation (4)

$$\begin{cases} M_1 = GJ_t\rho_1 + K\rho_2 \\ M_2 = EI_2\rho_2 + K\rho_1 \\ M_3 = EI_3\rho_3 \end{cases} \tag{4}$$

The curvatures ρ_1, ρ_2 and ρ_3 are described by Equation (5) according to [33]

$$\begin{cases} \rho_1 = \varphi' + v''w' \\ \rho_2 = -w'' + v''\varphi \\ \rho_3 = v'' + w''\varphi \end{cases} \tag{5}$$

The displacement variables are then defined as the sum of an equilibrium term denoted with the suffix 0 and a perturbation term as in Equation (6).

$$\begin{cases} \varphi = \varphi_0 + \tilde{\varphi} \\ w = w_0 + \tilde{w} \\ v = v_0 + \tilde{v} \end{cases} \tag{6}$$

Substituting Equation (6) into Equation (5) and neglecting the known equilibrium terms, Equation (5) becomes:

$$\begin{cases} \rho_1 = \tilde{\varphi}' + v_0''\tilde{w}' + w_0'\tilde{v}'' \\ \rho_2 = -\tilde{w}'' + v_0''\tilde{\varphi} + \varphi_0\tilde{v}'' \\ \rho_3 = -\tilde{v}'' + w_0''\tilde{\varphi} + \varphi_0\tilde{w}'' \end{cases} \tag{7}$$

Equation (7) can be derived to obtain the differential of the curvatures $\partial\rho_1$, $\partial\rho_2$ and $\partial\rho_3$ which can be substituted into Equation (3) to derive the deformed equilibrium configuration-dependent stiffness matrix by integration of Equation (3). Further detail on the derivation of the non-linear beam element stiffness matrix can be found in [35].

VI. Analysis Workflow

In this section, the analysis workflow is outlined. The aerodynamic analysis is performed with Athena Vortex Lattice (AVL). AVL is a software created by Mark Drela from MIT Aero & Astro and Harold Youngren. The software is based on the numerical method Vortex Lattice Method (VLM). VLM calculates lift curve slope, induced drag, and lift distribution for a given wing configuration. The wing is modeled with horseshoe vortices distributed along the span and chord. These vertices produce a lift according to four theories, Biot-Savart Law, Kutta-Joukovsky theorem, Herman von Helmholtz theory, and Prandtl lifting-line theory.

In this work, the objective is to obtain the aerodynamic loads acting on the wing surface and apply them to the structural linear or non-linear model. The deformation caused by the aerodynamic loads defines a new configuration with different geometry and incidence of the wing sections. The new geometry is then used as input for AVL to compute the new aerodynamic loads for a new iteration. The process stops when convergency is reached and the new loads do not change the geometry or when the incidence of the airfoils indicates that the aeroelastic divergence has been reached. The analysis workflow is illustrated in Figure 2.

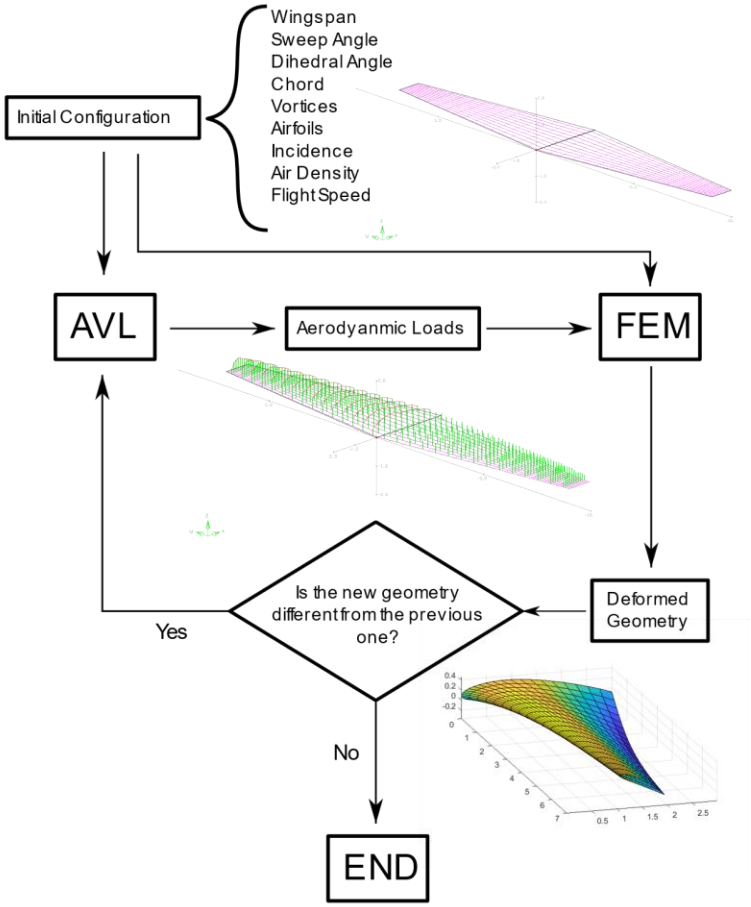

Fig. 2 Analysis workflow

VII. Aeroelastic Divergence of Stiffness Coupled Graphite/Epoxy Cantilever Plates

The test case chosen for the aeroelastic analysis procedure here presented consists of four graphite/epoxy cantilever plates with different fiber orientations. Hollowell and Dungundji [31] conducted an analytical and experimental investigation to determine the aeroelastic divergence behavior of unswept, rectangular wings simulated by graphite/epoxy, cantilevered plates with various bending-torsion stiffness coupling represented in Figure 3. The plates were laminated with a midplane symmetric stacking sequence, and the graphite/epoxy tape used for the experimental models was Hercules ASI/3501-6 with mechanical properties listed in Table 1, with the orthotropic engineering constants it is possible to obtain the off-axis lamina modulus components Q_{ij}.

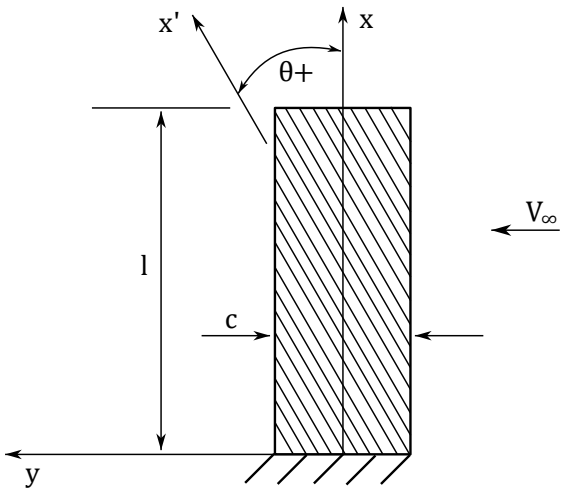

Fig. 3 Plate Layout

Table 1. Hercules ASI/3501-6

Property	In-plane loading	Out-of-plane loading
E_L [MPa]	130×10^3	98×10^3
E_T [MPa]	10.5×10^3	7.9×10^3
ν_{LT}	0.28	0.28
G_{LT} [MPa]	6.0×10^3	5.6×10^3
Ply Thickness [m]	0.134×10^{-3}	
Density [kg/m^3]	1520	

The laminate flexural and torsional stiffness can be obtained with Equation (8) according to [36], [37].

$$\begin{aligned} GJ_t &= 4l\left(D_{66} - \frac{D_{26}^2}{D_{22}}\right) \\ K &= 2l\left(D_{16} - \frac{D_{12}D_{26}}{D_{22}}\right) \\ EI_y &= l\left(D_{11} - \frac{D_{12}^2}{D_{22}}\right) \\ EI_z &= E_L\frac{l^3 t}{12} \end{aligned} \tag{8}$$

Where the flexural modulus D_{ij} for an n-play laminate with arbitrary ply angle orientation was obtained from Equation (9), l is the lamina length and t is the lamina total thickness.

$$D_{ij} = \sum_{k=1}^{n} Q_{ij}^{(\theta_k)} [z_k^3 - z_{k-1}^3]/3 \tag{9}$$

Where $Q_{ij}^{(\theta_k)}$ is the off-axis lamina modulus of the *k*th ply, θ_k the ply angle of the *k*th ply, and z_k the distance up from the midplane to the upper surface of the *k*th ply. The flexural moduli computed for the six laminates investigated are reported in Table 2.

Table 2. Flexural moduli for laminates [Nm] [31]

Laminate	D_{11}	D_{12}	D_{16}	D_{22}	D_{26}	D_{66}
$[0_2/90]_s$	4.125	0.096	0	0.490	0	0.243
$[\pm 45/0]_s$	1.550	0.928	0.437	1.404	0.437	1.075
$[-45_2/0]_s$	1.550	0.928	-0.946	1.404	-0.946	1.075
$[-30_2/0]_s$	2.704	0.720	-1.180	0.666	-0.459	0.866

The laminates represented in Figure 3 had an effective length *l* of 305 mm and a chord *c* of 76 mm for an aspect ratio *AR*=8. The total thickness was six plies. For the divergence analysis the lift curve slope $Cl_\alpha = \partial C_l/\partial\alpha = 2\pi$ has been empirically reduced with Equation (10) according to [38].

$$Cl_{\alpha_r} = Cl_\alpha * \frac{AR}{AR+2} \tag{10}$$

The BTCE model here presented can be used for the simulation of variable stiffness structures. In [30] different optimizations on curvilinear stiffener orientation have been performed to achieve specific structural performances. In this research work, the same idea has been applied to composite fiber orientation to show that curvilinear lamination can be adopted to improve the aeroelastic performance of a composite wing structure. At this scope, four simulations with different curvilinear laminations have been conducted. The fibers orientation varies linearly with Equation (11) with θ_1 denoting the angle at the first section of the beam and θ_2 the angle at the last section of the beam (Figure 4).

$$\theta(x) = \theta_1 + \frac{(\theta_2 - \theta_1)}{l} x \tag{11}$$

The reference case is the lamination $[-45_2/0]_s$ with $\theta_1 = \theta_2 = -45°$, then the orientation θ_1 is kept fixed at $-45°$ while orientation θ_2 is considered equals to $-30°$, $-10°$, $0°$, and $+10°$ for the different cases. Tip deflection and rotation are computed at different speeds to show the influence of curvilinear lamination on aeroelastic static analysis.

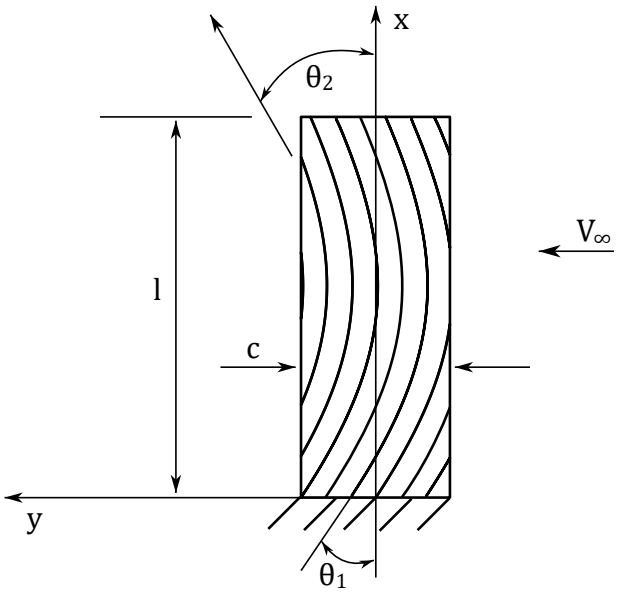

Fig. 4 Curvilinear Lamination

VIII. Results and Discussion

The results obtained are summarized in Table 3. The first three columns report the experimental and analytical results presented in [31], while the last two columns present the results obtained with the procedure here presented computed for $Cl_\alpha = 2\pi$ and for Cl_{α_r}.

Table 3. Divergence velocities [m/s]

Laminate	Experimental [31]	Analytical ($Cl_\alpha = 2\pi$) [31]	Analytical (Cl_{α_r}) [31]	BTCE ($Cl_\alpha = 2\pi$)	BTCE (Cl_{α_r})
$[0_2/90]_s$	flutter	22.3	25.0	22.62	24.34
$[\pm 45/0]_s$	>32.0	No divergence	No divergence	>32.0	>32.0
$[-45_2/0]_s$	12.5	9.9	11.1	11.56	12.44
$[-30_2/0]_s$	11.7	10.2	11.5	11.12	11.94

The laminations $[90/0]_s$, $[-45_2/0]_s$ and $[-30_2/0]_s$] which have a negative or null bending-torsion coefficient presented divergence at a certain speed. The plate with lamination $[0_2/90]_s$ can be used as a reference case, the plate has straight fibers and therefore bending, and torsion are uncoupled, during the experimental tests reported in [31] the specimen experienced flutter right before divergence and this affected the detection of the divergence velocities. However, as shown in Figure 5, the numerical results here presented are in accordance with the previously published analytical results. The lamination $[-45_2/0]_s$ correspond to a negative bending-torsion stiffness D_{16}, for this reason, the section of the beam increases the incidence when the aerodynamic loads cause a deflection. This coupling determines a reduction of the divergence speed with respect to the straight lamination as shown in Figure 6. The results present some differences if compared to the analytical divergence velocities, however, they seem to be more in agreement with the experimental evidence. The test case with lamination $[-30_2/0]_s$ has the most

negative bending-torsion stiffness D_{16} which reduce further the divergence velocity as shown in Figure 7. In this case, there is good accordance with both experimental and analytical results.

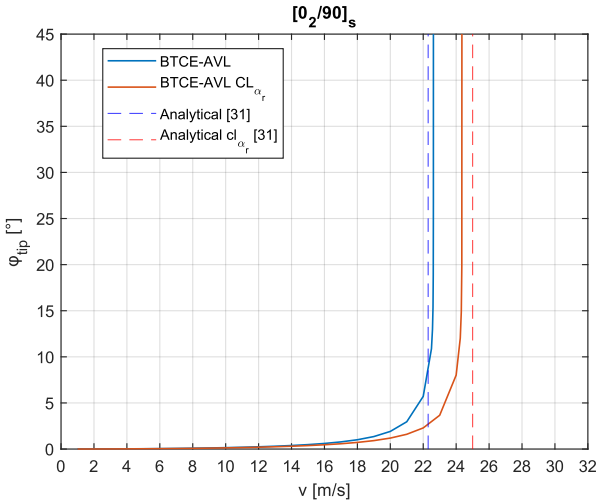

Fig. 5 Results Comparison plate $[0_2/90]_s$

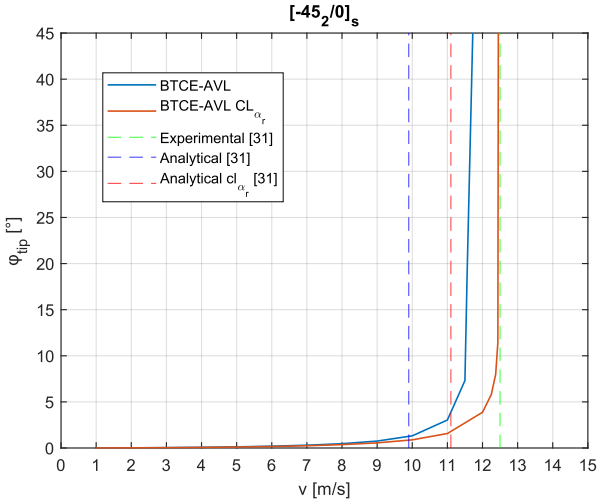

Fig. 6 Results Comparison plate $[-45_2/0]_s$

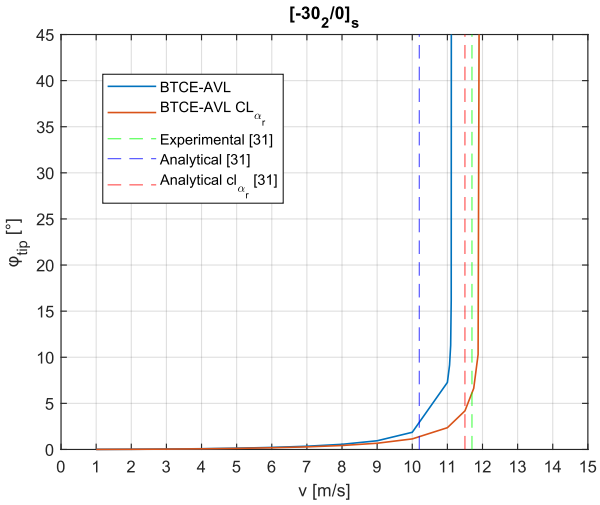

Fig. 7 Results Comparison plate $[-30_2/0]_s$

Hollowell published other experimental data in [39] concerning the tip deflection and the tip angle of attack of the lamination $[\pm 45/0]_s$ and $[-45_2/0]_s$ the results obtained with different initial angle of attack α_0 have been compared against the ones obtained with the BTCE model and are presented in Figures 8-11. For the lamination $[\pm 45/0]_s$ the results concerning the tip deflection are in good agreement with the experimental data, the deflection predicted with the BTCE model has a good level of accuracy even for high levels of deformation up to 50%. Some discrepancies are present in the case where $\alpha_0 = 6°$ for high deformations. The tip rotation predicted with the BTCE tends to decrease with the speed, while the experimental tip rotation remains constant or slightly increases.

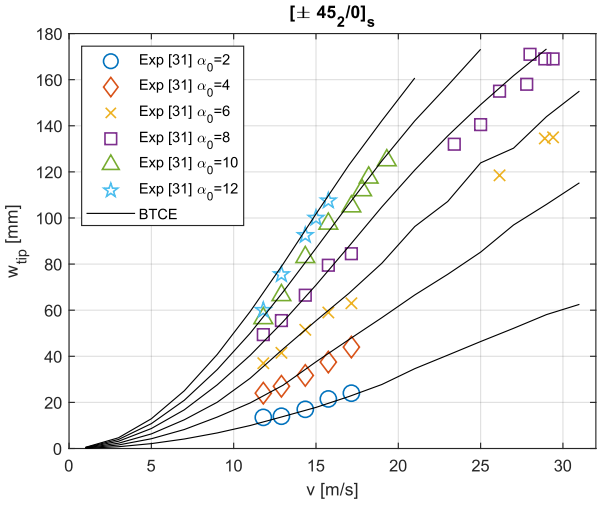

Fig. 8 Tip Deflection Results $[\pm 45/0]_s$

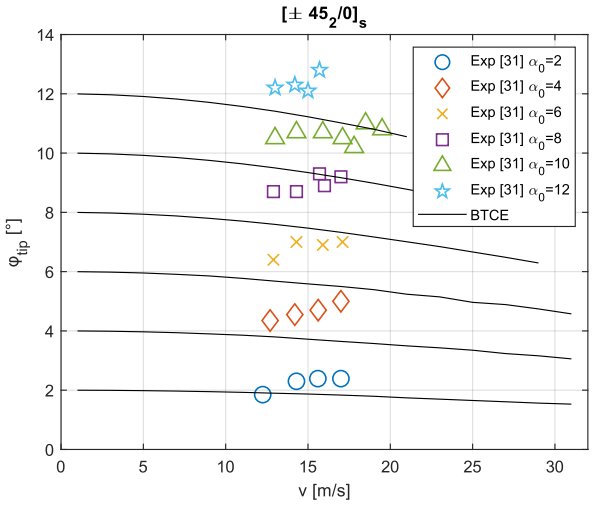

Fig. 9 Tip Rotation Results $[\pm 45/0]_s$

Divergent tendencies of both the tip lateral deflections and angle of attack for the $[-45/0]_s$ are apparent in Figures 10-11. The trend predicted with the BTCE model where similar to the experimental results presented in [39], however, the numerical and experimental results did not correlate. Finally, the numerical data appear to diverge faster than the experimental data.

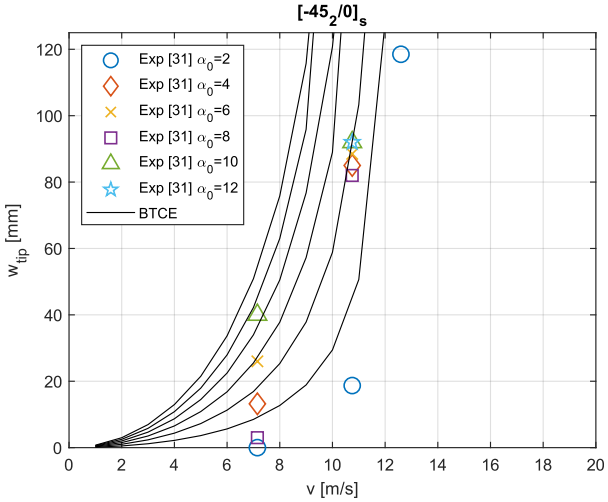

Fig. 10 Results Comparison plate $[\pm 45/0]_s$

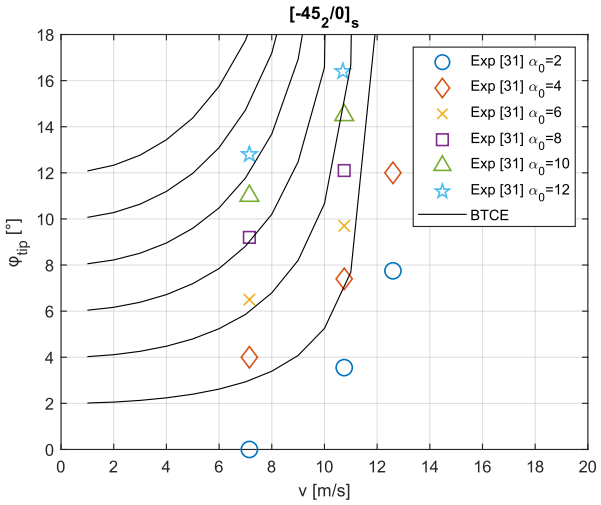

Fig. 11 Results Comparison plate $[-30_2/0]_s$

The numerical results for composite beam structure with curvilinear lamination are presented in Figures 12-13. It is possible to observe that the straight lamination $[-45_2/0]_s$ has the higher coupling effect showing divergence at low speed. When $\theta_2 = -30°$ The curvilinear path presents almost the same performance as the lamination $[-45_2/0]_s$, while for $\theta_2 = -10°$ and $\theta_2 = 0°$ the tip rotation and deflection increase slower and present a higher divergence velocity. For the case where $\theta_2 = 10°$ the coupling goes from negative to positive along the beam length, this causes a higher bending stiffness which results in a small deflection at a relatively high speed as shown in Figure 13. Moreover, the variable coupling keeps the tip rotation almost equal to zero for all the speeds considered as shown in Figure 12.

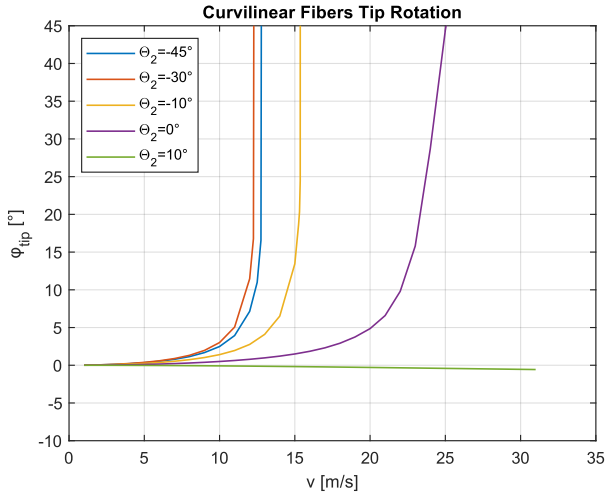

Fig. 12 Tip rotation results for different curvilinear laminations

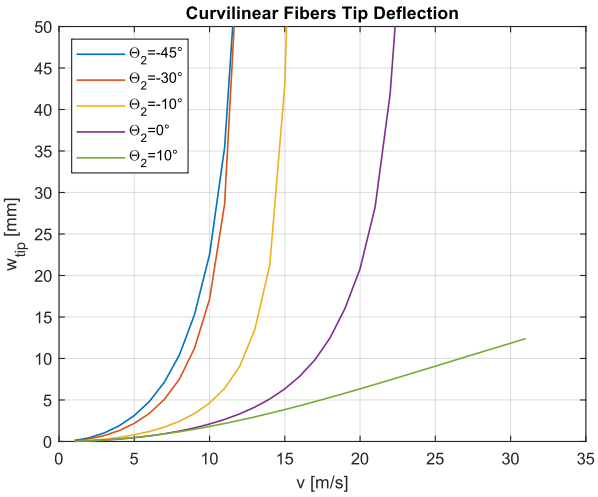

Fig. 13 Tip deflection results for different curvilinear laminations

IX. Conclusion

The present research work showed the capabilities of a beam finite element with bending torsion coupling formulation for static aeroelastic analysis. The procedure which involved a structural analysis by means of a BTCE model and an aerodynamic analysis based on VLM has been tested against experimental and analytical results presented in the literature. The divergence velocities predicted with the present method are in good agreement with experimental results, while tip deflection and rotation did not correlate with the experimental data in one of the tested cases. The procedure has been applied also to different curvilinear laminations to show their effects on the static aeroelastic analysis results and the possible application of the BTCE. The BTCE proved to be a versatile analysis tool that can be integrated into an aerodynamic analysis and can be used for static aeroelastic analysis, moreover, it can be combined with curvilinear lamination introducing design variables that can be used to achieve specific aeroelastic performance. The present methodology can be further developed with optimization algorithms for optimization problems and extended to flutter analysis.

Appendix A.

$$[K] = \begin{bmatrix} \frac{12EI_z}{L^3} & 0 & 0 & 0 & \frac{6EI_z}{L^2} & -\frac{12EI_z}{L^3} & 0 & 0 & 0 & \frac{6EI_z}{L^2} \\ 0 & K_1 & 0 & K_2 & 0 & 0 & -K_1 & 0 & K_2 & 0 \\ 0 & 0 & \frac{GJ_t}{L} & \frac{K}{L} & 0 & 0 & 0 & -\frac{GJ_t}{L} & -\frac{K}{L} & 0 \\ 0 & K_2 & \frac{K}{L} & K_3 & 0 & 0 & -K_2 & -\frac{K}{L} & K_4 & 0 \\ \frac{6EI_z}{L^2} & 0 & 0 & 0 & \frac{4EI_z}{L} & -\frac{6EI_z}{L^2} & 0 & 0 & 0 & \frac{2EI_z}{L} \\ -\frac{12EI_z}{L^3} & 0 & 0 & 0 & -\frac{6EI_z}{L^2} & \frac{12EI_z}{L^3} & 0 & 0 & 0 & -\frac{6EI_z}{L^2} \\ 0 & -K_1 & 0 & -K_2 & 0 & 0 & K_1 & 0 & -K_2 & 0 \\ 0 & 0 & -\frac{GJ_t}{L} & -\frac{K}{L} & 0 & 0 & 0 & \frac{GJ_t}{L} & \frac{K}{L} & 0 \\ 0 & K_2 & -\frac{K}{L} & K_4 & 0 & 0 & -K_2 & \frac{K}{L} & K_3 & 0 \\ \frac{6EI_z}{L^2} & 0 & 0 & 0 & \frac{2EI_z}{L} & -\frac{6EI_z}{L^2} & 0 & 0 & 0 & \frac{4EI_z}{L} \end{bmatrix} \quad \text{(A1)}$$

$$K_1 = \frac{12\left(EI_y GJ_t - K^2\right)}{GJ_t L^3} \quad K_2 = \frac{6\left(K^2 - EI_y GJ_t\right)}{GJ_t L^3}$$
$$K_3 = \frac{4EI_y GJ_t - 3K^2}{GJ_t L^3} \quad K_4 = \frac{4EI_y GJ_t - 3K^2}{GJ_t L^3} \tag{A2}$$

References

[1] G. Dimitriadis, *Introduction to nonlinear aeroelasticity*, 1 edition. Chichester, West Sussex, UK: Wiley, 2017.

[2] F. Afonso, J. Vale, É. Oliveira, F. Lau, e A. Suleman, «A review on non-linear aeroelasticity of high aspect-ratio wings», *Progress in Aerospace Sciences*, vol. 89, pp. 40–57, feb. 2017, doi: 10.1016/j.paerosci.2016.12.004.

[3] M. J. Patil e D. H. Hodges, «Flight Dynamics of Highly Flexible Flying Wings», *Journal of Aircraft*, vol. 43, fasc. 6, pp. 1790–1799, nov. 2006, doi: 10.2514/1.17640.

[4] E. Cestino, G. Frulla, E. Perotto, e P. Marzocca, «Experimental Slender Wing Model Design by the Application of Aeroelastic Scaling Laws», *J. Aerosp. Eng.*, vol. 27, fasc. 1, pp. 112–120, gen. 2014, doi: 10.1061/(ASCE)AS.1943-5525.0000211.

[5] M. J. Patil e D. H. Hodges, «On the importance of aerodynamic and structural geometrical nonlinearities in aeroelastic behavior of high-aspect-ratio wings», *Journal of Fluids and Structures*, vol. 19, fasc. 7, pp. 905–915, ago. 2004, doi: 10.1016/j.jfluidstructs.2004.04.012.

[6] M. J. Patil, D. H. Hodges, e C. E. S. Cesnik, «Characterizing the Effects of Geometrical Nonlinearities on Aeroelastic Behavior of High-Aspect Ratio Wings», presentato al International Forum on Aeroelasticity and Structural Dynamics, 1999, pp. 501–510.

[7] V. C. Sherrer, T. J. Hertz, e M. H. Shirk, «Wind Tunnel Demonstration of Aeroelastic Tailoring Applied to Forward Swept Wings», *Journal of Aircraft*, vol. 18, fasc. 11, pp. 976–983, nov. 1981, doi: 10.2514/3.57589.

[8] S. Guo, «Aeroelastic optimization of an aerobatic aircraft wing structure», *Aerospace Science and Technology*, vol. 11, fasc. 5, pp. 396–404, giu. 2007, doi: 10.1016/j.ast.2007.01.003.

[9] L. Librescu e O. Song, «On the static aeroelastic tailoring of composite aircraft swept wings modelled as thin-walled beam structures», *Composites Engineering*, vol. 2, fasc. 5–7, pp. 497–512, gen. 1992, doi: 10.1016/0961-9526(92)90039-9.

[10] D. Li, C. Gong, A. Da Ronch, G. Chen, e Y. Li, «An efficient implementation of aeroelastic tailoring based on efficient computational fluid dynamics-based reduced order model», *Journal of Fluids and Structures*, vol. 84, pp. 182–198, gen. 2019, doi: 10.1016/j.jfluidstructs.2018.10.011.

[11] D. H. Hodges, «Geometrically Exact, Intrinsic Theory for Dynamics of Curved and Twisted Anisotropic Beams», *AIAA Journal*, vol. 41, fasc. 6, pp. 1131–1137, giu. 2003, doi: 10.2514/2.2054.

[12] D. H. Hodges, «A mixed variational formulation based on exact intrinsic equations for dynamics of moving beams», *International Journal of Solids and Structures*, vol. 26, fasc. 11, pp. 1253–1273, 1990, doi: 10.1016/0020-7683(90)90060-9.

[13] M. Drela, «Integrated simulation model for preliminary aerodynamic, structural, and control-law design of aircraft», in *40th Structures, Structural Dynamics, and Materials Conference and Exhibit*, St. Louis,MO,U.S.A.: American Institute of Aeronautics and Astronautics, apr. 1999. doi: 10.2514/6.1999-1394.

[14] M. Ritter, J. Jones, e C. E. Cesnik, «Enhanced Modal Approach for Free-flight Nonlinear Aeroelastic Simulation of Very Flexible Aircraft», in *15th Dynamics Specialists Conference*, San Diego, California, USA: American Institute of Aeronautics and Astronautics, gen. 2016. doi: 10.2514/6.2016-1794.

[15] R. R. Medeiros, C. E. S. Cesnik, e E. B. Coetzee, «Computational Aeroelasticity Using Modal-Based Structural Nonlinear Analysis», *AIAA Journal*, vol. 58, fasc. 1, pp. 362–371, gen. 2020, doi: 10.2514/1.J058593.

[16] B. Stanford, C. D. Wieseman, e C. Jutte, «Aeroelastic Tailoring of Transport Wings Including Transonic Flutter Constraints», in *56th AIAA/ASCE/AHS/ASC Structures, Structural Dynamics, and Materials Conference*, Kissimmee, Florida: American Institute of Aeronautics and Astronautics, gen. 2015. doi: 10.2514/6.2015-1127.

[17] M. H. Shirk, T. J. Hertz, e T. A. Weisshaar, «Aeroelastic tailoring - Theory, practice, and promise», *Journal of Aircraft*, vol. 23, fasc. 1, pp. 6–18, gen. 1986, doi: 10.2514/3.45260.

[18] C. L. Pettit e R. V. Grandhi, «Optimization of a Wing Structure for Gust Response and Aileron Effectiveness», *Journal of Aircraft*, vol. 40, fasc. 6, pp. 1185–1191, nov. 2003, doi: 10.2514/2.7208.

[19] P. D. Dunning, B. K. Stanford, H. A. Kim, e C. V. Jutte, «Aeroelastic tailoring of a plate wing with functionally graded materials», *Journal of Fluids and Structures*, vol. 51, pp. 292–312, nov. 2014, doi: 10.1016/j.jfluidstructs.2014.09.008.
[20] L. Librescu e K. Maalawi, «Material grading for improved aeroelastic stability in composite wings», *JOMMS*, vol. 2, fasc. 7, pp. 1381–1394, set. 2007, doi: 10.2140/jomms.2007.2.1381.
[21] M. W. Tosh e D. W. Kelly, «On the design, manufacture and testing of trajectorial fibre steering for carbon fibre composite laminates», *Composites Part A: Applied Science and Manufacturing*, vol. 31, fasc. 10, pp. 1047–1060, ott. 2000, doi: 10.1016/S1359-835X(00)00063-4.
[22] C. Wu, Z. Gurdal, e J. Starnes, «Structural Response of Compression-Loaded, Tow-Placed, Variable Stiffness Panels», in *43rd AIAA/ASME/ASCE/AHS/ASC Structures, Structural Dynamics, and Materials Conference*, Denver, Colorado: American Institute of Aeronautics and Astronautics, apr. 2002. doi: 10.2514/6.2002-1512.
[23] R. Kapania, J. Li, e H. Kapoor, «Optimal Design of Unitized Panels with Curvilinear Stiffeners», in *AIAA 5th ATIO and16th Lighter-Than-Air Sys Tech. and Balloon Systems Conferences*, Arlington, Virginia: American Institute of Aeronautics and Astronautics, set. 2005. doi: 10.2514/6.2005-7482.
[24] D. Locatelli, S. B. Mulani, e R. K. Kapania, «Wing-Box Weight Optimization Using Curvilinear Spars and Ribs (SpaRibs)», *Journal of Aircraft*, vol. 48, fasc. 5, pp. 1671–1684, set. 2011, doi: 10.2514/1.C031336.
[25] L. O. Bernhammer, R. D. Breuker, e M. Karpel, «Geometrically Nonlinear Structural Modal Analysis Using Fictitious Masses», *AIAA Journal*, vol. 55, fasc. 10, pp. 3584–3593, ott. 2017, doi: 10.2514/1.J054787.
[26] E. Kantor, D. E. Raveh, e R. Cavallaro, «Nonlinear Structural, Nonlinear Aerodynamic Model for Static Aeroelastic Problems», *AIAA Journal*, vol. 57, fasc. 5, pp. 2158–2170, mag. 2019, doi: 10.2514/1.J057309.
[27] A. Drachinsky e D. E. Raveh, «Modal Rotations: A Modal-Based Method for Large Structural Deformations of Slender Bodies», *AIAA Journal*, vol. 58, fasc. 7, pp. 3159–3173, lug. 2020, doi: 10.2514/1.J058899.
[28] C. Patuelli, E. Cestino, e G. Frulla, «A Beam Finite Element for Static and Dynamic Analysis of Composite and Stiffened Structures with Bending-Torsion Coupling», *Aerospace*, vol. 10, fasc. 2, p. 142, feb. 2023, doi: 10.3390/aerospace10020142.
[29] C. Patuelli, A. Polla, E. Cestino, e G. Frulla, «Experimental and Numerical Dynamic Behavior of Bending-Torsion Coupled Box-Beam», *J. Vib. Eng. Technol.*, nov. 2022, doi: 10.1007/s42417-022-00759-7.
[30] C. Patuelli, E. Cestino, G. Frulla, e F. Valente, «Optimization of Curvilinear Stiffener Beam Structures Simulated by Beam Finite Elements with Coupled Bending–Torsion Formulation», *Materials*, vol. 16, fasc. 9, p. 3391, apr. 2023, doi: 10.3390/ma16093391.
[31] S. J. Hollowell e J. Dugundji, «Aeroelastic flutter and divergence of stiffness coupled, graphite/epoxy cantilevered plates», *Journal of Aircraft*, vol. 21, fasc. 1, pp. 69–76, gen. 1984, doi: 10.2514/3.48224.
[32] E. Cestino e G. Frulla, «Analysis of slender thin-walled anisotropic box-beams including local stiffness and coupling effects», *Aircraft Eng & Aerospace Tech*, vol. 86, fasc. 4, pp. 345–355, lug. 2014, doi: 10.1108/AEAT-10-2012-0159.
[33] A. H. Nayfeh e P. F. Pai, *Linear and Nonlinear Structural Mechanics*, 1ª ed. Wiley, 2004. doi: 10.1002/9783527617562.
[34] M. R. M. Crespo da Silva e C. C. Glynn, «Nonlinear Flexural-Flexural-Torsional Dynamics of Inextensional Beams. I. Equations of Motion», *Journal of Structural Mechanics*, vol. 6, fasc. 4, pp. 437–448, gen. 1978, doi: 10.1080/03601217808907348.
[35] C. Patuelli, E. Cestino, e G. Frulla, «A Non-Linear Beam Finite Element with Bending-Torsion Coupling Formulation for Dynamic Analysis with Geometric Nonlinearities», *International Journal of Non-Linear Mechanics*, (to be published).
[36] M. R. Kramer, Z. Liu, e Y. L. Young, «Free vibration of cantilevered composite plates in air and in water», *Composite Structures*, vol. 95, pp. 254–263, gen. 2013, doi: 10.1016/j.compstruct.2012.07.017.
[37] T. A. Weisshaar e B. L. Foist, «Vibration tailoring of advanced composite lifting surfaces», *Journal of Aircraft*, vol. 22, fasc. 2, pp. 141–147, feb. 1985, doi: 10.2514/3.45098.
[38] R. L. Bisplinghoff, H. Ashley, e R. L. Halfman, *Aeroelasticity*. in Dover science books. New York: Dover, 1996.
[39] S. J. Hollowell, «Aeroelastic flutter and divergence of graphite/epoxy cantilevered plates with bending-torsion stiffness coupling», Thesis (M.S.), Massachusetts Institute of Technology. Dept. of Aeronautics and Astronautics.